Isı Bilimi ve Tekniği Dergisi,42, 2, 203-220, 2022
J. of Thermal Science and Technology

ISSN 1300-3615
https://doi.org/10.47480/isibted.1194986

# THEORETICAL AND EXPERIMENTAL INVESTIGATION OF V-CORRUGATED SOLAR AIR HEATER FOR SPACE HEATING

**Murat ÖZDENEFE* and Khaled ALTEER ****
* Eastern Mediterranean University, Department of Mechanical Engineering
Gazimağusa, North Cyprus via Mersin 10, Turkey
murat.ozdenefe@emu.edu.tr, ORCID: 0000-0002-8905-0885
** Vocational Technical Institute, Technical Affairs, and Equipment Unit
AL-smalia st, Algarabolli, Tripoli, Libya
alteer22111@gmail.com, ORCID: 0000-0001-6379-8054

(Geliş Tarihi: 05.02.2022, Kabul Tarihi: 23.08.2022)

**Abstract**: This work is an effort to investigate the thermal performance of a V-Corrugated Solar Air Heater (SAH), which is intended for supplying heating to an office space having a floor area of 84 $m^2$. Thermal performance investigation has been carried out both theoretically and experimentally. V-Corrugated SAHs have not been investigated for space heating in offices, hence this study aims to contribute by proposing and promoting them for this purpose. The load of the office space has been evaluated by the Energy Plus building simulation program as 4546 W. Thermal performance of the SAH is investigated by solving the governing equations with developed MATLAB code and concurrently by carrying out real-time monitoring of the operating parameters (e.g. component temperatures, air speed, etc.) of the SAH. It is aimed to obtain the temperature of each component of the SAH, useful heat output, thermal efficiency, number of SAHs and the corresponding area that is necessary to meet the heating load. It is found that 9 SAHs with 16 $m^2$ are required to supply the target load for the experimental case and 6 SAHs with 10 $m^2$ for the theoretical case.
**Keywords**: V-Corrugated solar air heater, Thermal performance, Heating load simulation, Energy Plus

# V-KAT LEVHALI GÜNEŞ ENERJİLİ HAVA ISITICISININ ORTAM ISITMASI İÇİN TEORİK VE DENEYSEL İNCELEMESİ

**Özet**: Bu çalışma, 84 $m^2$ alana sahip bir ofise ısıtma sağlamak için tasarlanan V-Kat levhalı güneş enerjili hava ısıtıcısının ısıl performansını incelemektedir. Hava ısıtıcısının ısıl performansı hem teorik hem de deneysel olarak incelenmiştir. V-Kat levhalı güneş enerjili hava ısıtıcıları daha önce ofislere ısıtma sağlamak için çalışılmamıştır. Dolayısıyla bu çalışma bu sistemleri bu amaç için inceleyerek literatüre katkı sunmayı hedeflemektedir. Ofisin ısıtma yükü, Energy Plus bina simülasyon yazılımı ile 4546 W olarak hesaplanmıştır. Hava ısıtıcısının ısıl performansı, hava ısıtıcısı enerji denklemlerinin geliştirilen MATLAB kodu kullanılarak çözülmesi ile ve aynı zamanda hava ısıtıcısı işletme değişkenlerinin (örn. bileşen sıcaklıkları, hava hızı vb.) ölçülmesi ile incelenmiştir. Hava ısıtıcısının her bir bileşeninin sıcaklığı, faydalı ısı üretimi, ısıl verim, ısıtma yükünü karşılamak için gerekli olan hava ısıtıcısı sayısı ve karşılık gelen alanın elde edilmesi amaçlanmaktadır. Deneysel incelemenin sonucunda ısıtma yükünü karşılamak için 16 $m^2$ lik 9 adet hava ısıtıcısı gerekirken, teorik incelemede yükü karşılamak için10 $m^2$ lik 6 adet hava ısıtıcısının gerekli olduğu sonucu ortaya çıkmıştır.
**Anahtar Kelimler**: V-Kat levhalı güneş enerjili hava ısıtıcısı, Isıl performans, Isıtma yükü simülasyonu, Energy Plus

## NOMENCLATURE

| | | | |
|---|---|---|---|
| Aa | Absorber surface area [$m^2$] | A2 | Cross-sectional area-lower channel [$m^2$] |
| Ah | SAH Area [$m^2$] | Cp | Specific heat of air [J/kg.K] |
| A1 | Cross-sectional area-upper channel [$m^2$] | Dh | Hydraulic diameter [m] |
| | | G | Solar irradiance [W/$m^2$] |
| | | H | Thickness [m] |

| | |
|---|---|
| h | Heat transfer coefficient [$W/m^2$ .K] |
| k | Thermal conductivity [W/m .K] |
| L | Length of SAH [m] |
| $\dot{m}$ | mass flow rate [kg/s] |
| N | Number of SAH |
| Nu | Nusselt number [=hL/k] |
| Pr | Prandtl number |
| Qu | Total useful heat [W] |
| $Q_{htg}$ | Heating load of the office space [W] |
| qu1 | Useful heat from upper channel [W] |
| qu2 | Useful heat from lower channel [W] |
| R | Back elements resistance [m.K/W] |
| Ra | Rayleigh number [$=g\beta Pr(T_1-T_2)L^3/\nu^2$] |
| Re | Reynolds number [$=V\rho D/\mu$] |
| T | Temperature [K] |
| V | Velocity/Wind speed [m/s] |

**Greek letters**

| | |
|---|---|
| α | Absorptance |
| τ | Transmittance |
| σ | Stefan Boltzmann constant [$W/m^2$. $K^4$] |
| β | Thermal expansion coefficient [1/K] |
| ε | Emissivity |
| ν | Dynamic viscosity [$m^2/s$] |
| θ | Tilt angle [°] |
| η | Thermal efficiency |
| μ | Dynamic viscosity [kg/m·s] |
| ρ | Density [$kg/m^3$] |

**Subscripts:**

| | |
|---|---|
| 1 | Upper channel |
| 2 | Lower channel |
| a | Ambient air |
| ap | Absorber plate |
| bp/b | Back plate |
| c | Convection |
| Exp | Experimental |
| f1 | Air flow in upper channel |
| f2 | Air flow in lower channel |
| g1 | Upper glass cover |
| g2 | Lower glass cover |
| i & o | Inlet & Outlet |
| ins | Insulation |
| pc | Protective cover |
| r | Radiation |
| s | Sky |
| Sim | Simulation |
| w | wind |

## INTRODUCTION

Solar energy collectors are devices that convert solar radiation to useful thermal energy by absorbing the incident radiation, transforming it to heat, and transferring the heat to the working fluid (water, oil, air, etc.). Solar air heaters (SAHs) are solar energy collectors employing air as the working fluid. Unlike solar water heaters (working fluid is water) where the conduits are pipes, SAHs utilize ducts for transporting the working fluid i.e., air (Duffie John A. et al., 2020; Kalogirou, 2004).

A generic SAH consists of a transparent cover system, an absorber plate, and insulated air ducts/channels. The cover system is at the top, whereas the absorber plate commonly is above the air ducts/channels. A portion of the incident radiation on the cover system is transmitted and falls on the absorber plate where it is absorbed. The remaining on the other hand is reflected. The air which flows either naturally by buoyancy force (passive SAH) or by an external force (active SAH with a fan) exchanges heat with the absorber plate by convection and can be used for different purposes such as space heating or drying of crops. Thermal performance of SAHs depends on many variables such as dimensions of SAH, absorber plate type and material, amount of solar radiation, the geometry of the air ducts and the amount of air flow, etc.

### Motivation

Although SAHs are simple and cheap, their real-life applications for space heating are not very common. Indeed, they possess a vast potential for space heating in locations with moderate climates having abundant solar radiation. For instance, the Mediterranean region could be ideal for employing SAHs for space heating.

Buildings are responsible for one-third of the world's end use energy consumption. This makes them the second largest energy-consuming sector after industrial sector. They also account for 30% of global $CO_2$ emissions. Within the buildings, space heating end-use has the largest contribution to $CO_2$ emissions accounting for 60% (International Energy Agency, 2021).

It is apparent, that renewable technologies if employed for space heating can have an appreciable effect on end-use energy reduction and $CO_2$ mitigation. SAHs which currently have no widespread real-life applications can be considered one of those renewable technologies which are simple and inexpensive that can have a considerable

effect on reducing energy consumption and $CO_2$ emissions, particularly in locations where the climate is mild.

North Cyprus is an ideal place to be considered for space heating with SAHs, since the island has mild weather (Mediterranean Climate) with a yearly average temperature of 19 $^oC$ and average daily solar radiation of 17.5 $MJ/m^2$ (4.86 $kWh/m^2$) through the year. During winter the coldest month is January with daytime temperatures in the range of 9-12 $^oC$ and daily mean solar radiation of 9.0 $MJ/m^2$ (2.50 $kWh/m^2$) (North Cyprus Meteorological Office, 2022).

Commercial buildings in North Cyprus accounted for 36% of the total electricity consumption in 2021 (kıb-tek, 2021). These buildings are mainly offices, and they heavily rely on electricity-powered heat pumps for space heating during winter. Considering that electricity production in North Cyprus relies on fuel oil-driven power plants, facilitating the real-life applications of SAHs for space heating would have a significant impact on reducing energy and greenhouse gas emissions.

Hence, the principal motivation of the current work is to propose and promote the SAHs, particularly the V-Corrugated absorber plate type, through investigating its thermal performance for office heating applications under North Cyprus weather conditions.

**Literature Review**

There has been extensive research on the SAHs. Numerous models have been developed for examining their performance and many configurations have been tested for different applications some of which are presented below.

Yıldırım and Solmuş (2014) numerically investigated a double glass double pass SAH. The authors aimed to find the duct depth and air flow rate that would give the maximum thermohydraulic efficiency. They revealed that the maximum thermohydraulic efficiency occurred as 67% with a duct depth of 4 cm and an air flow rate of 0.11 kg/s. The authors also found that the daily mean thermal efficiency of the SAH decreases with increasing air duct depth.

Al-Kayiem and Yassen (2015) compared the theoretically evaluated Nusselt numbers (Nu) with those obtained experimentally for a flat plate glass covered SAH for different tilt angles under natural convection conditions. The authors found that some theoretical models overestimate, whereas some others underestimate the Nu. They also revealed that the optimum tilt angle is about 50$^o$ for obtaining the highest Nusselt number.

Bayrak and Oztop (2015) experimentally tested flat plate SAHs which are incorporated with Aluminum foam obstacles with different arrangements. The authors revealed that the SAH with 6 mm thick Aluminum foam obstacles having staggered arrangement has the highest efficiency as 77%.

Gawande et al. (2016) investigated the effect of L-shaped roughness elements which are introduced reversely on the absorber plate of a SAH. The authors performed CFD simulations (with ANSYS Fluent) and compared their results with experimental measurements. They found that introducing the roughness elements substantially affects the heat transfer characteristics. They also revealed that optimum heat transfer enhancement is with a thermo-hydraulic performance parameter of 1.90 and the CFD simulations are agreeing with experimental results.

Gilani et al. (2017) experimentally examined the Nu number enhancement of natural convection SAHs by installing conical-shaped turbulators. The authors observed that the staggered arranged turbulators with a height of 4 mm and a pitch of 16 mm increased the Nu number the most.

Gao et al. (2000) solved the governing equations (continuity, momentum and energy) in order to investigate the parameters effecting natural convection in a sine wave absorber plate cross corrugated SAH. They found that the channel height to the amplitude of the sine wave shaped absorber plate ratio and one-fourth of the sine wave shaped absorber plate wavelength to the amplitude of the sine wave shaped absorber plate should be greater than 2 and 1 respectively, whereas the tilt angle should be less than 40$^o$ to suppress the natural convection heat loss.

El-Sebaii et al. (2011) theoretically and experimentally investigated the double-pass finned-absorber plate and double-pass V-Corrugated absorber plate SAHs. The authors observed that the double-pass V-Corrugated absorber plate SAH exit air temperature and efficiency are 2.1-9.7% and 9.3-11.9% greater than the double-pass finned-absorber plate SAH's exit air temperature and efficiency. The authors also found that both solar air heater's efficiencies are increasing up to a mass flow rate

of 0.04 kg/s which beyond this value efficiency enhancement is insignificant.

Kumar A. et al. (2022) proposed a novel counter flow curved double-pass solar air heater (DPSAH). The authors performed CFD analysis and experimentally validate their results with those available in the literature. They also compared the results of smooth curved single pass, smooth curved parallel double-pass, smooth curved counter double-pass, roughened curved parallel double-pass, and roughened curved counter double-pass. The authors found that roughened curved counter double-pass has the best performance with a maximum of 23% increase in the thermal performance.

In another study, Jain and Jain (2004) investigated the performance of a multi-pass flat absorber plate SAH having a granite storage material attached to the back of the absorber plate which is intended for drying paddy crops. The authors solved the energy equations and calculated the temperatures of the air at different locations in the SAH as well as the paddy grain temperature. They have found that increasing the SAH length and breadth increases paddy grain temperature.

Another experimental drying application (for roselle) of a SAH is examined by Kareem et al. (2017) The authors investigated the drying performance of a multi-pass flat plate SAH integrated with granite for heat storage. Their design achieved a drying rate of 33.57 g $(kg\ m^2\ h)^{-1}$ with an efficiency of 64%. The systems' techno-economic appraisal resulted in a payback period of 2.14 years.

A more recent work regarding the use of the SAHs as a dryer is done by Çiftçi et al. (2021) The authors developed a vertical photovoltaic thermal (PVT) solar dryer and performed numerical and experimental investigation (for drying mint). They considered the system with and without fins. The authors revealed that the thermal efficiency of the system without fins and with fins could be as high as 54.86% and 58.16% respectively. They also found that waste exergy ratios of the system without fins and with fins are in the ranges of 0.47-0.58 and 0.43-0.56 respectively.

Fan et al. (2017) developed a dynamic model for a hybrid photovoltaic thermal collector solar air heater (PVT-SAH) which is equipped with longitudinal fins for evaluating system performance. The authors validated their model with an experimental study under real-life conditions. They measured the temperatures of the system components at various points and compared them with those evaluated with the model and found that the root-mean-square deviation ranges from 0.3 to 1.3 ºC.

In another study, Fan et al. (2019a) designed a model for a PV thermal solar air heater (PVT-SAH) system integrated with heat pipes whose SAH portion is a double pass type with longitudinal fins. The system is intended to generate high-temperature air. The authors evaluated the thermal efficiency of the proposed system as 69.2% and payback time in the range of 5.7 and 16.8 years (Fan et al., 2019a).

In a study subsequent to aforementioned one, Fan et al (2019b) employed the PVT-SAH for the regeneration process of a desiccant cooling system. The authors applied the developed system to a commercial building having offices for cooling which is in a hot and humid climate. The authors found that the COP of the system can be as high as 19.8 and a minimum area of 0.35 $m^2$ PVT-SAH is necessary per $m^2$ of the conditioned floor area to go above the typical COPs (2.6-3.0).

Agathokleous et al. (2019) developed a dynamic simulation model which was implemented through MATLAB for simulating the energy performance of building integrated, vertically installed multi-pass serpentine type flat plate SAH. The authors also investigated the thermal comfort of the occupants and performed an economic analysis of the system. The authors tested the prototype of the SAH and performed simulations of the proposed system for an office building with a 200 $m^2$ floor area for three different locations. The authors found that space heating savings could be as much as 3.4 MWh/y.

Prakash et al. (2022) investigated the energy and exergy performance of double pass hybrid SAH with sensible heat storage material (Metco and aluminum scrap mixture) which was placed underneath the backplate of the system. The authors tested the system for three different operation modes: natural convection mode, forced convection mode, and forced convection mode with a reflector. The forced convection mode with a reflector performed best with energy and exergy efficiencies of 86.19% and 17.617% respectively. The authors concluded that the system is suitable for space heating, desalination, drying, and other industrial and domestic applications.

**Research Gap and Contribution of the Current Work**

Although there has been broad research on SAHs, notable real-life applications of these systems to offices for space heating and performance testing are very few. It has been presented in the literature review that Fan et al. (2019b) and Agathokleous et al. (2019) developed, tested, and considered SAHs for offices. However, the system developed by Fan et al. is for producing heated air which is intended to be used in the regeneration process of a desiccant cooling system that supplies cooling to a commercial building. The work done by Agathokleous et al. on the other hand is intended for office heating, though the SAHs are building integrated, vertically installed and are multi-pass serpentine type.

To the best knowledge of the authors, real-life performance testing and application of a V-Corrugated SAH for space heating of offices do not exist. Hence, the current study will contribute to the literature by filling this gap. The objectives of the work can be summarized as (1) to evaluate the heating load of the selected office, (2) to model the V-Corrugated SAH for evaluating component temperatures, useful heat, efficiency, and area required to cover the load, (3) to experimentally test the SAH and compare the theoretical results with the test results.

**Structure of the Paper**

This work comprises five sections: Introduction, Methodology, Results & Discussion, Uncertainty Analysis and Conclusion. The Introduction section involves the motivation for the study, a review of the state of art of SAHs, and the contribution of the current work to the literature. The Methodology section elaborates on the materials and methods that are followed to realize the objectives of the study. First, the office space in consideration is described and subsequently its load evaluation is explained. Then the mathematical model of the V-Corrugated SAH is presented. Lastly Experimental procedure is elaborated. Results of the theoretical and experimental approach are presented and discussed in the Results & Discussion section. A brief uncertainty analysis is performed under the Uncertainty Analysis section. The Conclusion section at the end presents the principal findings of the study and concluding remarks.

**METHODOLOGY**

In this study, previously manufactured V-Corrugated SAH (Sahebari *et al.*, 2013) is retrofitted and installed to supply heat to an office space (Alteer, 2017). It is intended to evaluate the required number and area of SAHs that will cover the heating demand for a typical winter day. The performance of the system is investigated theoretically (through the solution of the mathematical model of the SAH by developed MATLAB code) and experimentally and the results are compared. Energy Plus software is utilized to estimate the heating load of the office space which is necessary for evaluating the required number and area of SAH.

The SAH employed in this study is a type with two glass covers and an absorber plate that is in V-Corrugated shape. The air flows through the series of channels having equilateral cross-section areas that are formed by the V-Corrugated absorber plate and the lover glass cover/back plate. Figure 1 illustrates the cross-section and the main components of the V-Corrugated SAH that is considered in this study. The principal advantages of the V corrugations are the increase in the absorber plate area and the enhancement of the convection heat transfer coefficient due to the corrugated shape which also positively affects the radiative characteristics of the absorber plate (Sparrow and Lin, 1962).

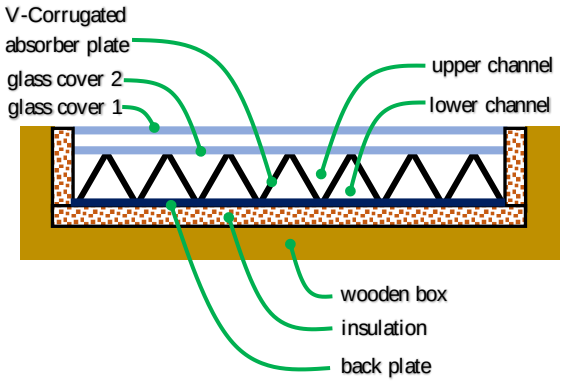


**Figure 1.** Cross section and the main components of the V-Corrugated SAH.

This work involves three principal segments: 1- load evaluation of the office space, 2- mathematical modelling and theoretical investigation of the SAH and 3- experimental investigation of the SAH.

The load of the office space is evaluated by Energy Plus program whereas the mathematical model of the SAH (energy balance equations of each component of SAH) is solved by the MATLAB program for associated

temperatures and useful heat output. Theoretically evaluated useful heat output (from MATLAB) is used together with the load of the office space to find the number of SAHs and area that are necessary to meet the heating demand of the space during a typical winter day. The SAH is also investigated experimentally. Temperature measurements of the SAH components together with the environmental variables (ambient temperature, solar radiation, and wind speed) have been taken and used to evaluate the actual useful heat output from the SAH.

The outputs of the MATLAB program have been compared with the experimental results to reveal the difference between the actual and model performance of the SAH. The methodology which has been followed in this work is schematically illustrated in Figure 2.

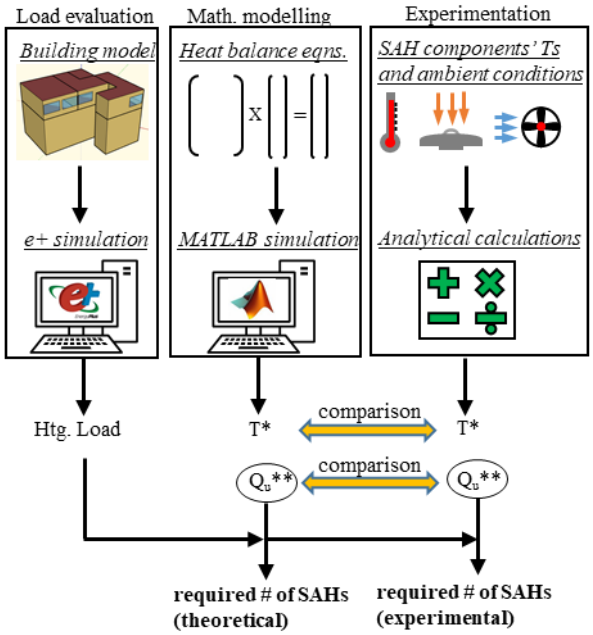


**Figure 2.** Methodology (*: SAH components' temperatures, **: Useful energy output from SAH).

## Load Evaluation

The Energy Plus program is the tool employed for evaluating the heating load of the office space. The program is a dynamic energy and load simulation engine which is for energy appraisal and heating/cooling load calculations of buildings. It has been developed by the US Department of Energy and comes with components for constructing input files (IDF editor) and running processes (EP-launch). Energy Plus is made up from various modules which are designed for modeling and simulating applications such as pumping power calculations, conduction heat transfer evaluations through building fabric, heating/cooling coil computations, etc. In addition to the modelling/simulation modules, there are other files and auxiliary programs that can be fed to and embedded into Energy Plus such as weather data files, example files generator and 3D ground heat transfer tool that enable a proper building energy simulation (U.S. Department of Energy, 2016a; 2016b; 2016c).

The office space that is intended to be served by the SAH is the Mechanical Engineering Department chairperson's office located at the top floor of the Mechanical Engineering Department building at the Eastern Mediterranean University campus in North Cyprus, Famagusta. The office space has a floor area of 84 $m^2$ and is made up from the construction materials that are widely used in North Cyprus. Figure 3 presents the plan of the office space, whereas Figure 4 shows the 3D model of the office space generated and to be exported to the Energy Plus program. The construction materials' properties that are entered into the program are given in Table **1** (ASHRAE, 2017; CIBSE, 2015; Turkish Standards Institute, 2008).

Indoor air temperature of 20°C is assumed for the space, whereas the outdoor conditions of the city of Larnaca (Lat. 34.9°, Lon. 33.6°) are employed for the load calculations since Famagusta's weather data does not exist in the Energy Plus. The meteorological conditions of Famagusta and Larnaca are very similar as two locations lie on the cost only about 50 km away from each other and have almost identical geographical features. The outdoor design temperature is 3.8°C.

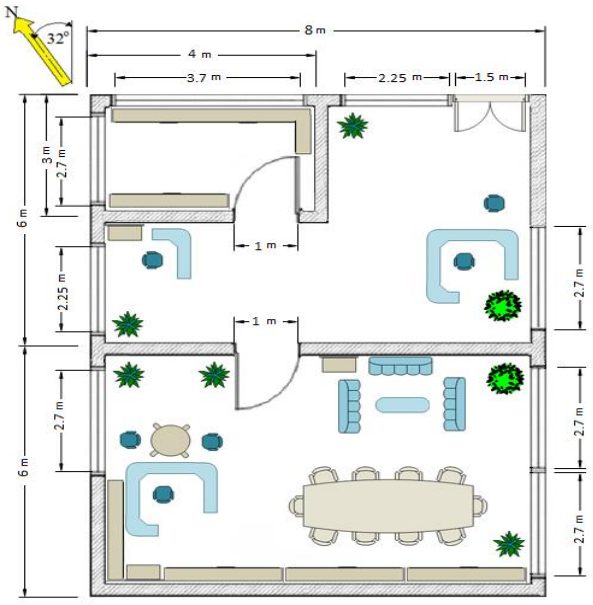


**Figure 3.** Office space to be served by SAH.

**Table 1.** Properties of the construction materials (ASHRAE, 2017; CIBSE, 2015; Turkish Standards Institute, 2008).

| Struct. | Material & thickness | k (W/m.K) | ρ (kg/m$^3$) | $c_p$ (J/kg.K) |
|---|---|---|---|---|
| Walls | Cement 2.5 cm | 1.4 | 2100 | 650 |
| | Brick 25 cm | 0.4 | 700 | 840 |
| | Cement 2.5 cm | 1.4 | 2100 | 650 |
| Floor | Marble 2 cm | 2.9 | 2750 | 840 |
| | Screed 1.5 cm | 1.4 | 2100 | 650 |
| | RC 20 cm | 2.1 | 2400 | 840 |
| | Cement 2.5 cm | 1.4 | 2100 | 650 |
| Roof | Screed 5 cm | 1.4 | 2100 | 650 |
| | RC 20 cm | 2.1 | 2400 | 840 |
| | Cement 2.5 cm | 1.4 | 2100 | 650 |
| Doors | Hardwood | 0.17 | 700 | 1880 |
| Windows' U values are 3.2 W/m$^2$.K<br>RC: reinforced concrete | | | | |

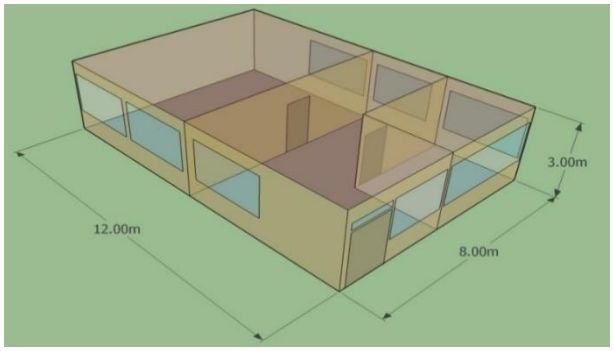


**Figure 4.** 3D model of the office space that is exported to Energy Plus for load evaluation.

## Mathematical Model

As emphasized in the preceding sections it is intended to estimate the number and area of SAHs that is necessary to supply the amount of heat required to cover the load of the office space during a typical winter design day. To do that useful heat (Qu) output from the SAH is to be evaluated theoretically. $Q_u$ can be evaluated by multiplying the capacity rate of the air (mass flow rate times the specific heat of the air) with the inlet-outlet air temperature difference through the SAH. Specific heat of air is known, and a mass flow rate can be set. However, the outlet air temperature of the SAH should be evaluated. This requires the calculation of temperatures of each constituent (e.g., glass, absorber plate, air layer, etc.) of the SAH. Associated temperatures of the SAH are obtained by deriving the energy balance equations (algebraic equations) for each component separately and forming a matrix to be solved for each component's as well as air layers' temperature simultaneously.

The components of the SAH are two flat transparent glasses i.e., glass 1 and glass 2, a V-Corrugated absorber plate, a flat back plate, and back elements (insulation, back wood, and galvanized steel protective cover). The list of these components from top to down and their dimensions are given in Table 2. The cross-section of the SAH is as shown in Figure 1 and the side and top views are as in Figure 5.

**Table 2.** SAH components and dimensions (from top to down).

| Component | Material | Dimensions |
|---|---|---|
| Transparent cover 1 & 2 | Glass | 94 cm x 194 cm 0.4 cm thick |
| V- Corrug. absorber plate | Galvanized steel dyed in black | Corrug. angle 60° 0.2 cm thick |
| Back plate | Galvanized steel | 97 cm x 197 cm 0.2 cm thick |
| Back insulation | Polystyrene | 97 cm x 197 cm 2 cm thick |
| Back wood | Balsa wood | 100 cm x 200 cm 4 cm thick |
| Protective cover | Galvanized steel | 100 cm x 200 cm 0.2 cm thick |

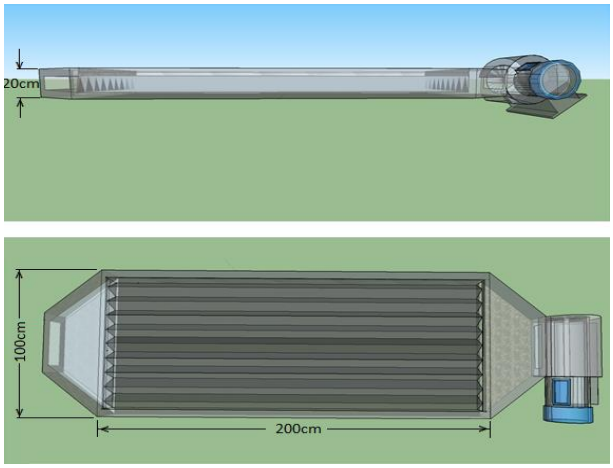


**Figure 5.** Side and top view of the SAH.

The equations of energy balance are constructed based on the thermal resistance network of the SAH which is

shown in Figure 6. Heat loss from the first cover occurs via forced convection (due to wind) and radiation to the ambient air and sky respectively. Thus, between the first cover and ambient air, there is forced convection resistance and there exists radiation resistance between the first cover and the sky. These two resistances are parallel to each other. Natural convection and radiation heat exchange take place across the second and first cover resulting in natural convection and radiation resistances in parallel. The absorbed radiation by the V-Corrugated absorber plate is distributed to the second glass cover and bottom plate by radiation and to the air flows in the upper and lower channels via forced convection. In addition, the flowing air in the upper and lower channels loses heat to the second glass cover and back plate respectively by forced convection. This results in a series of forced convection resistances connected to radiation resistance in parallel in the upper and lower channels. There exists heat loss across the back of the SAH which is via conduction through the back elements and convection from the outer surface. These are represented by a single resistance. The mathematical model of the SAH is based on the following assumptions (Lin *et al.*, 2006; Liu *et al.*, 2007):

- Steady-state conditions prevail
- Heat flow through the back elements is 1D
- The thermal inertia of SAH components is neglected
- Both air channels are free of leakage
- During operation, temperatures of each component are uniform
- The sky is considered as a blackbody for long wavelength radiation at an equivalent sky temperature
- Heat loss through the front and back side of the collector is to the same ambient temperature
- The shading generated by the V-Corrugated absorber plate, dirt, and dust on the glass covers are negligible
- Air temperature varies in the heat flux direction

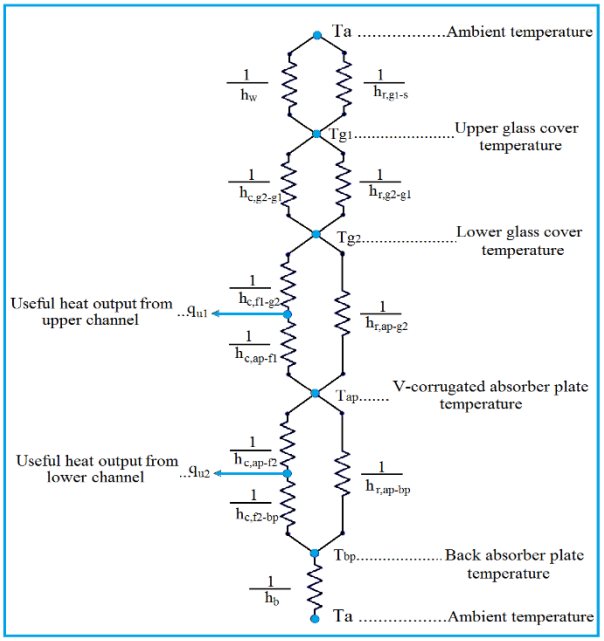


**Figure 6.** Thermal resistance network of the SAH.

The reasonings for the principal assumptions given above are elaborated as follows:

The mathematical model will be solved for each unknown parameter once at a time (once per hour) hence, assuming steady state is sufficient for the current study. In addition, the results would be presented hourly and within an hour in solar air heater applications, conditions can be presumed to be time-invariant. Since the considered SAH's back elements width (about 1 m) and length (about 2 m) are very large relative to the other dimension (thickness is about 0.062 m) and because the side wall areas of the SAH are very small it is reasonable to consider 1D heat transfer through the back elements. The thicknesses of the SAH components are very small (the thickest is the back wood with 0.04 m) hence the thermal storage of the components is neglected. Since the SAH's top and the bottom side is exposed to the same environment it is sufficient to assume that heat loss will be to the same temperature.

Equations (1) to (6) present energy balance equations for upper glass cover, lower glass cover, air in the upper channel, V-Corrugated absorber plate, air in the lower channel and back plate respectively (for description of abbreviations see the Symbols section) (Hedayatizadeh et al., 2016; Lin et al., 2006; Liu et al., 2007):

$$\alpha_{g1} G A_h + (h_{r,g2-g1} + h_{c,g2-g1})(T_{g2} - T_{g1}) A_h = h_w (T_{g1} - T_a) A_h + h_{r,g1-s} (T_{g1} - T_s) A_h \quad (1)$$

$$\tau_{g1}\alpha_{g2}GA_h + h_{r,ap-g2}\left(T_{ap} - T_{g2}\right)A_a + h_{c,\mathrm{f}1-g2}\left(T_{\mathrm{f}1} - T_{g2}\right)A_h = \left(h_{r,g2-g1} + h_{c,g2-g1}\right)(T_{g2} - T_{g1})A_h \quad (2)$$

$$h_{c,ap-\mathrm{f}1}\left(T_{ap} - T_{\mathrm{f}1}\right)A_a = \dot{q}_{u1} + h_{c,\mathrm{f}1-g2}(T_{\mathrm{f}1} - T_{g2})A_h \quad (3)$$

$$\tau_{g1}\tau_{g2}\alpha_{ap}GA_a = h_{r,ap-g2}\left(T_{ap} - T_{g2}\right)A_a + h_{c,ap-\mathrm{f}1}\left(T_{ap} - T_{\mathrm{f}1}\right)A_a + h_{c,ap-\mathrm{f}2}\left(T_{ap} - T_{\mathrm{f}2}\right)A_a + h_{r,pa-bp}(T_{ap} - T_{bp})A_a \quad (4)$$

$$h_{c,ap-\mathrm{f}2}\left(T_{ap} - T_{\mathrm{f}2}\right)A_a = \dot{q}_{u2} + h_{c,\mathrm{f}2-bp}\left(T_{\mathrm{f}2} - T_{bp}\right)A_h \quad (5)$$

$$h_{r,ap-bp}\left(T_{ap} - T_{bp}\right) + h_{c,\mathrm{f}2-bp}\left(T_{\mathrm{f}2} - T_{bp}\right) = h_b(T_{bp} - T_a) \quad (6)$$

Each of the above equations is arranged in the general form of the equation (7) where A, B, C, D, E, and F are factors in terms of convection and radiation coefficients, SAH and absorber plate area as well as air's capacity rate. Those equations can be written in the matrix multiplication form as [A]x[T]=[B]. [A] is a matrix that is made up from the coefficients of the temperatures of the elements (glass 1, glass 2, air, etc.) of the SAH. [T] is the column matrix which is made up from the temperature values of the elements of the SAH. [B] is also a column matrix that is formulated by using the heat transfer coefficients, environmental parameters, and thermophysical properties of the elements. The resulting matrix multiplication form is shown in Figure 7.

$$T_{g1}A + T_{g2}B + T_{f1}C + T_{ap}D + T_{f2}E + T_{bp}F = G \quad (7)$$

$$\begin{bmatrix} (h_{r,g2-g1}+h_{c,g2-g1}+h_w+h_{r,g1-s}) & -(h_{r,g2-g1}+h_{c,g2-g1}) & 0 & 0 & 0 & 0 \\ -(h_{r,g2-g1}+h_{c,g2-g1})A_h & (h_{r,ap-g2}A_a+(h_{c,f1-g2}+h_{r,g2-g1}+h_{c,g2-g1})A_h) & -(h_{c,f1-g2})A_h & -(h_{r,ap-g2}A_a) & 0 & 0 \\ 0 & -(h_{c,f1-g2})A_h & h_{c,ap-f1}A_a+\dot{m}c_p+h_{c,f1-g2}A_h & -(h_{c,ap-f1})A_a & 0 & 0 \\ 0 & -(h_{r,ap-g2})A_a & -(h_{c,ap-f1})A_a & (h_{r,ap-g2}+h_{c,ap-f1}+h_{c,ap-f2}+h_{r,ap-bp})A_a & -(h_{c,ap-f2})A_a & -(h_{r,ap-bp}A_a) \\ 0 & 0 & 0 & -(h_{c,ap-f2})A_a & (h_{c,ap-f2}A_a+\dot{m}c_p+h_{c,f2-bp}A_h) & -(h_{c,f2-bp}A_h) \\ 0 & 0 & 0 & -(h_{r,ap-bp}) & -(h_{c,f2-bp}) & (h_b+h_{r,ap-bp}+h_{c,f2-bp}) \end{bmatrix} * \begin{bmatrix} T_{g1} \\ T_{g2} \\ T_{f1} \\ T_{ap} \\ T_{f2} \\ T_{bp} \end{bmatrix} = \begin{bmatrix} (\alpha_{g1}G+h_wT_a+h_{r,g1-s}T_s) \\ (\tau_{g1}\alpha_{g2}GA_h) \\ (\dot{m}c_pT_a) \\ (\tau_{g1}\tau_{g2}\alpha_{ap}GA_h) \\ (\dot{m}c_pT_a) \\ (h_bT_{bp}) \end{bmatrix}$$

**Figure 7.** Matrix multiplication form of the energy balance equations.

Heat transfer coefficients associated with the SAH are elaborated below (Duffie *et al.*, 2020; Hedayatizadeh *et al.*, 2016; Lin *et al.*, 2006; Liu *et al.*, 2007).

Convection heat transfer coefficient between the glass cover 1 (upper glass cover) and the wind as well as radiation heat transfer coefficient between the glass cover 1 and sky is as follows (Duffie *et al.*, 2020):

$$h_w = 2.8 + 3V_w \quad (8)$$

$$h_{r,g1-s} = \sigma\varepsilon_{g1}(T_{g1} + T_s)(T_{g1}^2 + T_s^2) \quad (9)$$

The sky temperature (Ts) can be calculated by the expression given below (Hedayatizadeh et al., 2016):

$$T_s = T_a - 6 \quad (10)$$

Natural convection and radiation heat transfer coefficients across glass cover 1 and glass cover 2 are expressed as (Duffie *et al.*, 2020):

$$h_{c,g2-g1} = Nu_{g1-g2}\frac{k}{L} \quad (11)$$

$$h_{r,g2-g1} = \frac{\sigma(T_{g1}^2 + T_{g2}^2)(T_{g1} + T_{g2})}{1/\varepsilon_{g1} + 1/\varepsilon_{g2} - 1} \quad (12)$$

where $Nu_{g1\text{-}g2}$ is the Nusselt number across the covers. Since the tilt angle of the SAH in the current work is 45°, the following equation applies to the Nusselt number. Note that the * indicates that only positive values in the brackets will be used (Duffie et al., 2020).

$$Nu_{g1-g2} = 1 + 1.44\left[1 - \frac{1708}{Ra.cos\,\theta}\right]^*\left[1 - \frac{1708(sin\,1.8.\theta)^{1.6}}{Ra.cos\,\theta}\right] + \left[\left(\frac{Ra.cos\,\theta}{5830}\right)^{\frac{1}{3}} - 1\right]^* \quad (13)$$

Forced convection heat transfer coefficient between the air in the upper channel and the V-Corrugated absorber plate as well as the radiation heat transfer coefficient across the V-Corrugated absorber plate and the glass cover 2 (lower glass cover) is given below (Hedayatizadeh *et al.*, 2016):

$$h_{c,ap-f1} = Nu_{ap-f1}\frac{k_1}{D_h} \quad (14)$$

$$h_{r,ap-g2} = \frac{\sigma\varepsilon_{g2}\varepsilon_{ap}\left(T_{ap}^2 + T_{g2}^2\right)\left(T_{ap} + T_{g2}\right)}{\varepsilon_{g2} + \varepsilon_{ap} - \varepsilon_{ap}\varepsilon_{g2}} \quad (15)$$

$Nu_{ap\text{-}f1}$ is the Nusselt number in the upper channel and is given in the following equation. In the present work the Reynolds number (Re) of the flow in the upper channel is 8200 (2800 <Re=8208< 10000) hence the flow is transitional flow. Thus, the expression given below is for a transitional flow regime (Liu *et al.*, 2007).

$$Nu_{ap-f1} = 1.9 \times 10^{-6} Re_1^{1.79} + 225\frac{H_1}{L} \quad (16)$$

The forced convection heat transfer coefficient between the air in the lower channel and the back plate as well as the radiation heat transfer coefficient across the V-Corrugated absorber plate and the back plate are analogous to equation 14 and 15.

In the preceding equations where properties of air i.e., density, thermal conductivity, and dynamic viscosity, are necessary and following expressions can be used respectively (Lin et al., 2006):

$$\rho = 3.9147 - 0.016082T_f + 2.9013 \times 10^{-5}T_f^2 - 1.9407 \times 10^{-8} \times T_f^3 \quad (17)$$

$$k = (0.0015215 + 0.097459T_f - 3.3322 \times 10^{-5}T_f^2) \times 10^{-3} \quad (18)$$

$$\mu = (1.6157 + 0.06523T_f - 3.0297 \times 10^{-5}T_f^2)10^{-6} \quad (19)$$

The overall heat transfer coefficient of the back elements is calculated by the following equation:

$$h_b = \left(\frac{H_{bp}}{k_{bp}} + \frac{H_{ins}}{k_{ins}} + \frac{H_{wood}}{k_{wood}} + \frac{H_{pc}}{k_{pc}} + \frac{1}{h_w}\right)^{-1} \quad (20)$$

A MATLAB code is constructed to calculate the required number and area of SAH to cover the heating load of the office space. The code solves the linear heat balance equations that are expressed in the form of [A]x[T]=[B] by using the matrix inversion method. It evaluates the SAH components' temperatures simultaneously. Then the code calculates the exit temperature of the air from the upper and lower channels ($T_{f1o}$ and $T_{f2o}$) of the SAH by inserting the evaluated upper and lower channel fluid temperature values ($T_{f1}$ and $T_{f2}$) into the following equations. Note that it has been assumed that the air temperatures in the channels are the average of the inlet (ambient air temperature) and the outlet air temperatures:

$$T_{f1o} = 2T_{f1} - T_a \quad (21)$$

$$T_{f2o} = 2T_{f2} - T_a \quad (22)$$

Subsequently, the code evaluates the useful heat from the upper and lower air channels, total useful heat from the SAH and thermal efficiency respectively by the following equations:

$$q_{u1} = \dot{m}c_p(T_{f1o} - T_a)/2 \quad (23)$$

$$q_{u2} = \dot{m}c_p(T_{f2o} - T_a)/2 \quad (24)$$

$$Q_u = q_{u1} + q_{u2} \quad (25)$$

$$\eta = \frac{Q_u}{GA_h} \times 100 \quad (26)$$

Lastly, the number of collectors and total area required to cover the heating load of the office space are evaluated by the subsequent expressions:

$$N = \frac{Q_{htg}}{Q_u} \quad (27)$$

$$A_{total} = A_h N \quad (28)$$

Note that $Q_{htg}$ is the heating load of the office space that is calculated by Energy Plus and required to be inputted into the MATLAB code. Also, it should be stated that the thermophysical properties of the SAH and measured parameters/operating parameters (wind speed, ambient temperature, global solar radiation, air mass flow rate through SAH), with assumed initial temperatures of each component ($T_{g1}$, $T_{g2}$, $T_{f1}$, $T_{f2}$, $T_{ap}$, $T_{bp}$) are introduced into the code to determine all the initial values of heat transfer coefficients. Accordingly, the code obtains new temperature values for the new iteration, and this continues until the preset condition is satisfied. The flowchart illustrating the workflow of the MATLAB code is shown in Figure 8.

Table 3 on the other hand presents the thermophysical properties of the SAH that are entered into the MATLAB code.

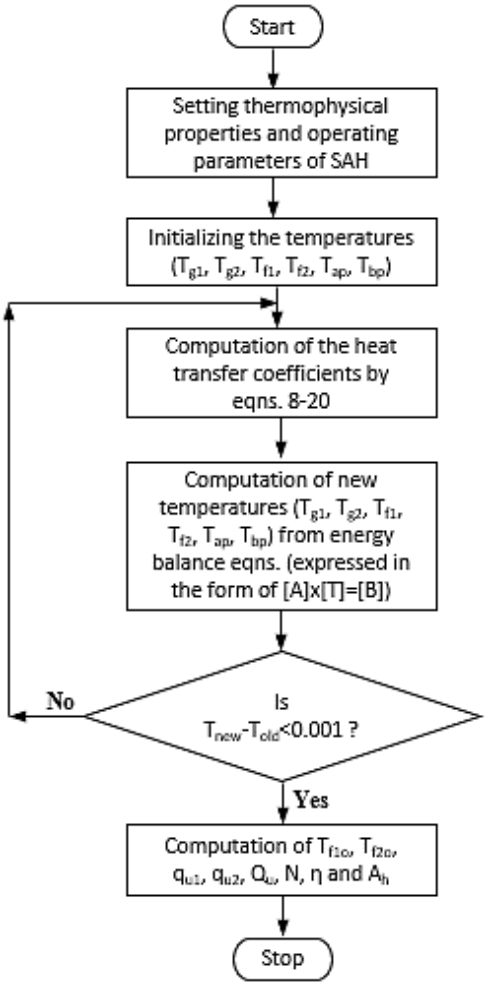


**Figure 8.** Workflow of the MATLAB code.

**Table 3:** Measured and thermophysical parameters required for the MATLAB code.

| Item: | SAH width | SAH length | g1 to g2 distance |
|---|---|---|---|
| Value: | 0.9 m | 1.94 m | 0.01 m |
| Item: | Height of the air channels | Back plate thickness | Insulation thickness |
| Value: | 0.1 m | 0.002 m | 0.02 m |
| Item: | Back wood thickness | Protective cover thickness | Back plate k |
| Value: | 0.04 m | 0.002 m | 80 W/m.K |
| Item: | Back wood k | Insulation k | Protective cover k |
| Value: | 0.1 W/m.K | 0.045 W/m.K | 80 W/m.K |
| Item: | $\alpha_{ap}$ | $\alpha_{g1}$ & $\alpha_{g2}$ | $\tau_{g1}$ & $\tau_{g2}$ |
| Value: | 0.9 | 0.06 | 0.9 |
| Item: | $\varepsilon_{g1}$ & $\varepsilon_{g2}$ | $\varepsilon_{ap}$ & $\varepsilon_{bp}$ | Tilt angle |
| Value: | 0.9 | 0.9 | 45° |
| Item: | Cp air | | |
| Value: | 1000 J/kg.K | | |

**Experimental Procedure**

Comparing the outputs of the MATLAB code for the various parameters ($T_{g1}$, $T_{g2}$, $T_{f1}$, $T_{f2}$, $T_{ap}$, $T_{bp}$) and the monitored values of the same parameters is one of the aims of this work. In this section, the experimental procedure is explained for monitoring the parameters that are used for comparison.

Various stages during the manufacturing of the V-Corrugated SAH (Sahebari *et al.*, 2013) are presented in Figure 9. As explained in the preceding section main components of the SAH are: two transparent glass covers, a V-Corrugated sheet metal absorber plate that is formed with groove angles of 60°, back absorber plate, polystyrene insulation, back wood, and protective cover. Air through the channels of the SAH is mobilized by an electric fan (type: OBR 200 M-2K) which is illustrated in Figure 10. The mass flow rate of the air is set by an electric resistor tool, which controls the input voltage in the range of 60 – 220 V.

**Figure 9.** Various stages of SAH manufacturing *(Sahebari et al.*, 2013).

**Figure 10.** Motor and fan of the SAH.

For recording the temperatures of each component of the SAH, ambient temperature, wind speed and air velocity from the SAH channels, the handheld data loggers Pasco Xplore GLX are used. These data loggers can be used with various sensors e.g., anemometer, temperature sensors, etc. Anemometer sensor (range: 0.5-29 m/s, accuracy: ± (3% of reading+ 0.2 m/s)) is employed for wind speed and air velocity measurements, whereas temperature sensors (range: from -30 °C to 105 °C, accuracy: ±0.5 °C) are used to measure ambient air temperature and temperatures of the SAH components. A pyranometer mounted on the SAH (linearity: ±0.5% from 0 to 2800 W/m$^2$) together with a data acquisition system, Omega OMB-DAQ-3000 is utilized to measure and log the global solar radiation incident on the SAH. The data acquisition system is connected to a desktop computer by a USB wire. The software package of the Data acquisition system is installed on this computer. Figure 11 shows the measuring/monitoring equipment

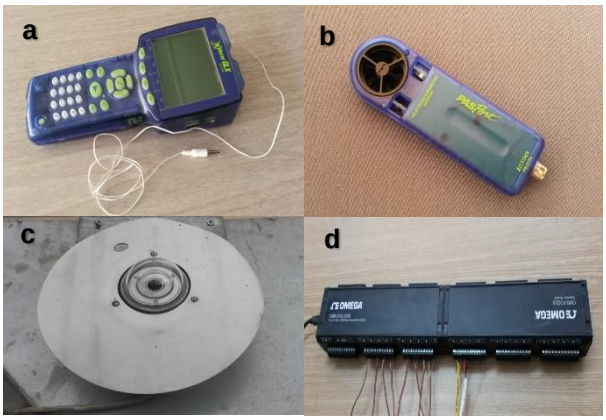


**Figure 11.** Measuring/monitoring equipment (a: handheld data logger and temperature sensor, b: anemometer, c: pyranometer and d: data acquisition system)

The SAH is tested at Famagusta, N. Cyprus (35.1°N and 33.9 °E). The surface azimuth of the collector is set as 0° thus; the collector is towards the south. The tilt angle of the collector is 45°. Figure 12 and Figure 13 illustrates the schematic and real view of the experimental setup. The measured wind speed is a required parameter in the MATLAB code for evaluating the convection heat transfer coefficient (see equation (**8**)) from the top and back of the SAH. Also, global solar radiation and air mass flow rate measurements are required parameters in the code for evaluating useful heat output. Equations (23), (24), (25), and (26) that are given in the preceding section are used to determine the useful heat from the upper air channel, the useful heat from the lower air channel, the total useful heat, and the thermal efficiency of the SAH experimentally.

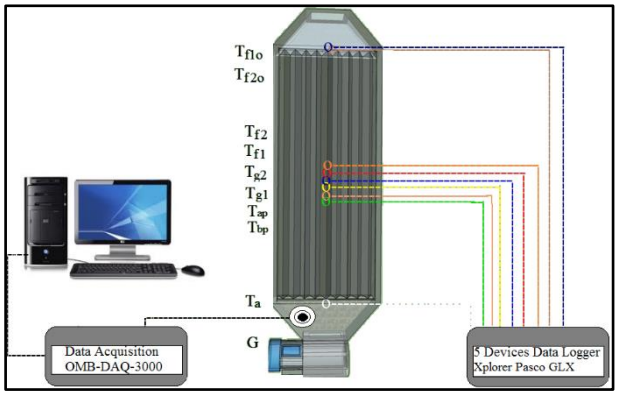


**Figure 12.** Schematic layout of the experimental setup.

**Figure 13.** View of the experimental setup.

## RESULTS AND DISCUSSION

The office space that is intended to be served by the SAH has been modeled and simulated by Energy Plus software to calculate the heating load. The simulation results revealed the space heating load as 4564 W.

To run the MATLAB code for evaluating the useful heat, thermal efficiency, etc. various environmental/operational parameters such as ambient/inlet air temperature ($T_a$), global solar radiation (G), wind speed ($V_w$), and air mass flow rate through the air duct are required to be inputted. These parameters have been monitored and recorded on 15$^{th}$ December throughout the times when the solar radiation is at its utmost level, from 11:00 until 14:30 for every 5 minutes (i.e. time step= 5 minutes). The mean of six values is evaluated for representing every half hour. Figure 14 presents the measured wind speed and global solar radiation incident on the SAH, whereas Figure 15 shows the measured ambient/inlet air temperature. The flow rate of the air is set according to the motor rpm. The motor rpm is adjusted to result in an air velocity of 1.8 m/s which gives a flow rate of 0.2 kg/s. With this flow rate, Reynolds numbers in the upper and lower channels are 8208 and 7579 respectively corresponding to the transitional flow regime in both channels.

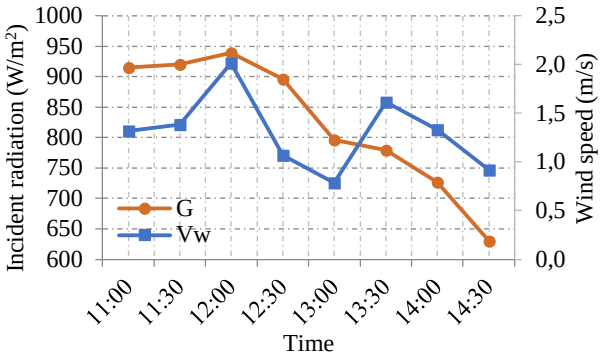


**Figure 14.** Measured wind speed and global solar radiation incident on SAH.

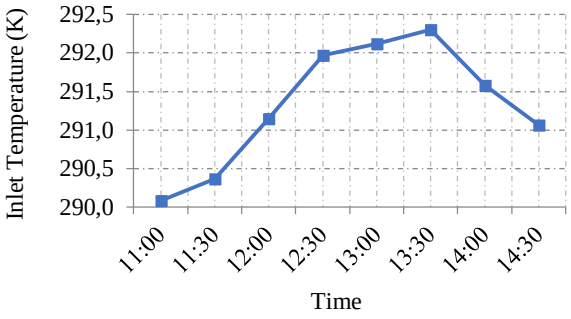


**Figure 15.** Measured ambient/inlet air temperature.

The temperature of the SAH elements; upper and lower glass cover, V-Corrugated absorber plate, and back plate are shown in Figure 16, Figure 17, Figure 18 and Figure 19 respectively.

When those figures are investigated, it is seen that the simulation results are having similar trends as the experimental ones. There is some discrepancy between the measured and simulated values. In some hours these discrepancies are very low whereas in some they are in significant order. The average of the differences of the simulated and monitored temperatures for upper glass cover, lower glass cover, V-Corrugated plate, and back plate are 1.4, 1.6, 2.8 and 2.0 K respectively.

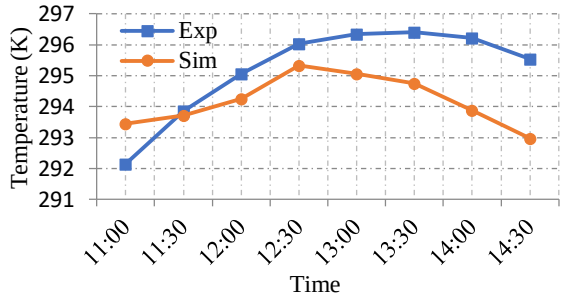


**Figure 16.** Upper glass cover temperatures.

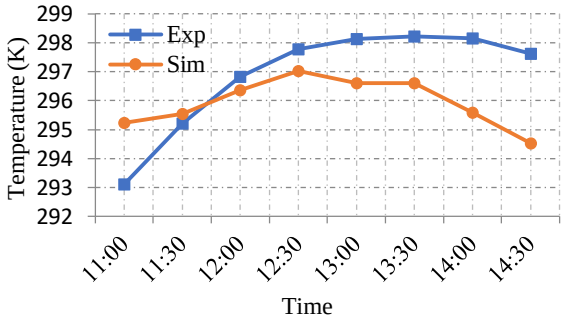


**Figure 17.** Lower glass cover temperatures.

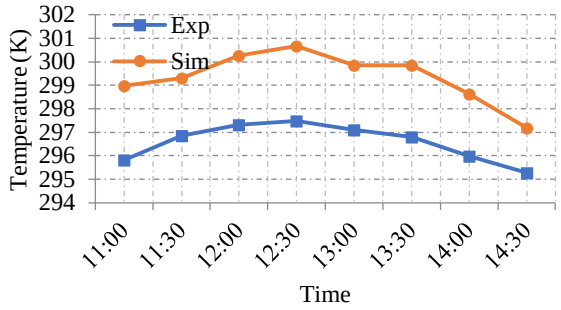


**Figure 18.** V-Corrugated absorber plate temperatures.

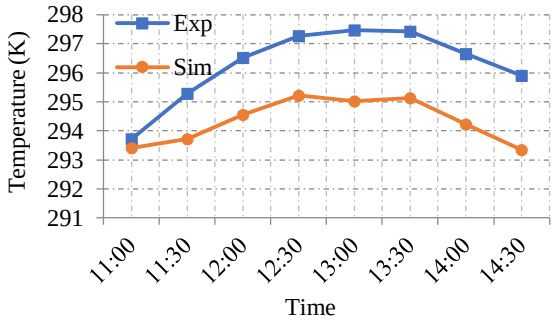


**Figure 19.** Back plate temperatures.

Air temperatures in the SAH; air temperature in the middle of the upper and lower channels as well as the air temperatures at the exit of the upper and lower channels are given in Figure 20, Figure 21, Figure 22, and Figure 23 respectively.

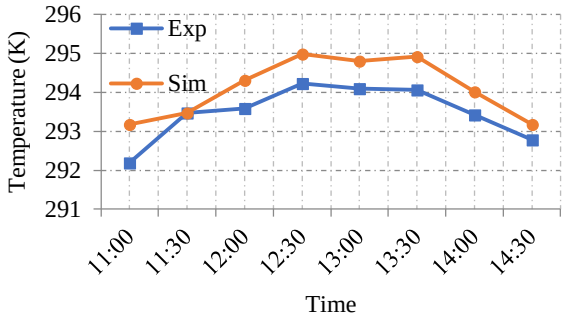


**Figure 20.** Air temperature at the middle of the upper channel.

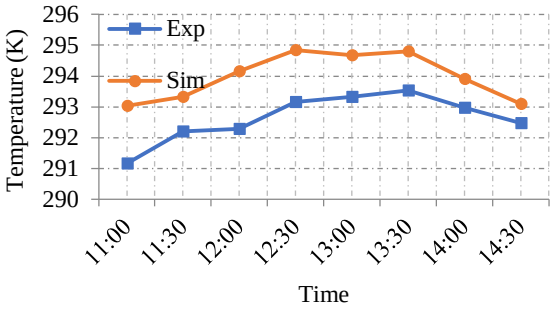


**Figure 21.** Air temperature at the middle of the lower channel.

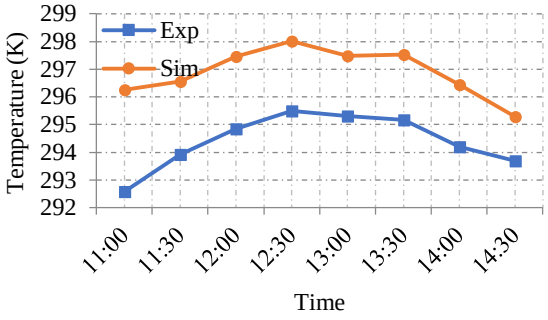


**Figure 22.** Air temperature at the exit of the upper channel.

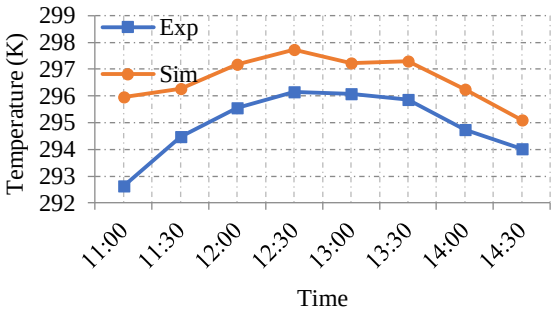


**Figure 23.** Air temperature at the exit of the lower channel.

Once the air temperatures at the middle and the exit of the upper and lower channels obtained from simulations and measurements are investigated, it is seen that the simulations and the measurements agree with some difference, however, the agreement is better than those for the SAH elements. The average of the differences between the measured and simulated values are 0.6, 1.3, 2.5, and 1.7 K for the air temperatures at the middle of

the upper channel, at the middle of the lower channel, at the exit of the upper channel, and at the exit of the lower channel respectively. The better agreement between the simulation results and the experimental measurements for the air temperatures than the SAH element temperatures is presumably due to the quick response of the air to the changes resulting in less effective dynamic behavior. It is expected to have some disagreement between the simulations and the measured values. First of all, the mathematical model that the MATLAB code is based on is not taking the thermal inertia and the dynamic behavior of the SAH into consideration (see the assumptions in the Mathematical model section). The response of the collector elements should be accounted to obtain more realistic results. In addition, the actual properties of the SAH components such as glass emissivity and transmissivity, absorber plate absorptivity, thermal conductivity, etc. are likely to have values that are different from those employed for MATLAB simulations. Although the values for these properties are found from reliable sources and catalogs, they may not match precisely with the actual values. Furthermore, the accuracies of the monitoring equipment are thought to influence the discrepancies.

Total useful heat output from the SAH and the thermal efficiency are shown in Figure 24 and Figure 25 respectively. The required number of SAHs and the area to meet the target heating load evaluated by the MATLAB code and the experimental analysis are shown in Table 4. Note that the values are given for every half hour. Number of SAH and corresponding area that is necessary to supply the load is taken as the max. number which resulted in 9 SAHs with 16 $m^2$ for the real case (experimental) and 6 SAHs with 10 $m^2$ for simulations.

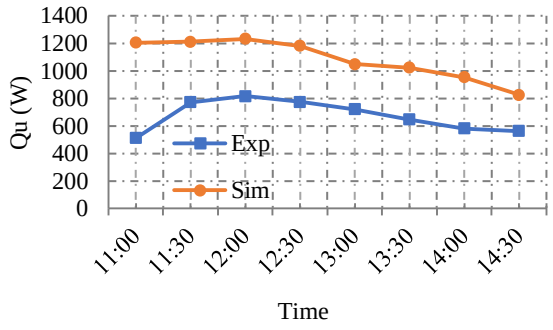


**Figure 24.** Useful heat from SAH.

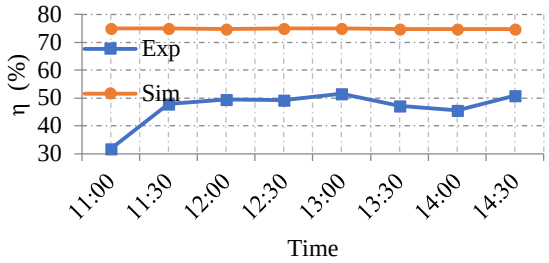


**Figure 25.** Thermal efficiency of the SAH.

**Table 4:** Required number of SAHs and area to meet the target heating load.

| Time | $\#_{exp}$ | $\#_{sim}$ | $Ah_{exp}$ ($m^2$) | $Ah_{sim}$ ($m^2$) |
|---|---|---|---|---|
| 11:00 | 8.9 | 3.8 | 15.6 | 6.6 |
| 11:30 | 5.9 | 3.8 | 10.4 | 6.6 |
| 12:00 | 5.6 | 3.7 | 9.8 | 6.5 |
| 12:30 | 5.9 | 3.9 | 10.3 | 6.8 |
| 13:00 | 6.3 | 4.4 | 11.1 | 7.6 |
| 13:30 | 7.1 | 4.5 | 12.4 | 7.8 |
| 14:00 | 7.8 | 4.8 | 13.8 | 8.4 |
| 14:30 | 8.1 | 5.5 | 14.2 | 9.7 |
| Max. | ≈ 9 | ≈ 6 | ≈ 16 | ≈ 10 |

## UNCERTAINTY ANALYSIS

Comparison of the obtained results by simulations and measurements revealed that, there are discrepancies between them. As stated in the preceding section one of the reason for this difference is believed to be because of the accuracies of the employed equipment in the experimentation. In this section an uncertainty analysis of the experimental results (for useful heat) is performed based on the following expression (Holman, 2012):

$$\omega_R = \left[\left\{\left(\frac{\partial R}{\partial x_1}\right)^2 \times \left(\omega_{x_1}\right)^2\right\} + \left\{\left(\frac{\partial R}{\partial x_2}\right)^2 \times \left(\omega_{x_2}\right)^2\right\} + \cdots + \left\{\left(\frac{\partial R}{\partial x_n}\right)^2 \times \left(\omega_{x_n}\right)^2\right\}\right]^{0.5} \quad (29)$$

Where R is a function of variables of $x_1$, $x_2$, … $x_n$, which its uncertainty is to be evaluated. $\omega_1$, $\omega_2$, … $\omega_n$ are the associated uncertainties of the variables and $\omega_R$ is the overall uncertainty of the function.

In the context of this study R is the Qu which its uncertainty will be evaluated and is function of the following measured variables:

- air temperature at the exit and inlet of the SAH
- air speed in the SAH

Note that Qu is evaluated by equation (25) which can be expanded as:

$$Q_u = \rho_1 A_1 V c_p \left(T_{f1o} - T_{f1i}\right) + \rho_2 A_2 V c_p \left(T_{f2o} - T_{f2i}\right) \quad (30)$$

It should be also noted that the air density is also function of temperature (see equation (17)).

Uncertainty of the Qu is evaluated by applying equation (29) together with the uncertainties of the air temperature and air speed measuring equipment ( ±0.5 °C and ± 3% of reading + 0.2 m/s, see subsection "Experimental Procedure") and it is found that the average of the uncertainty of the Qu throughout the day is 25.6% (Alteer, 2017).

## CONCLUSION

The principal aim of the present work is to investigate the performance of a V-Corrugated absorber plate SAH which is intended to be used in an office for space heating during a typical winter day in N. Cyprus. Although there are many studies on SAHs, space heating applications with them are few. Besides, to the knowledge of the authors, there are no V-Corrugated SAH applications for offices for space heating. Hence this study aims to contribute by proposing and promoting them for this purpose via thermal performance investigation. The performance of SAH is investigated theoretically and experimentally and the below outcomes are achieved:
The first phase of the work is to estimate the heating load of the office space in consideration by using Energy Plus software. The simulations gave the heating load as 4564 W.

The second outcome of this work is the number of SAHs and the area necessary to cover the load of the office space. This is achieved by evaluating the thermal performance of the SAH. Thermal performance is investigated theoretically and experimentally under the same environmental parameters that are obtained on 15$^{th}$ of December, from 11:00 until 14:30. The number of SAHs and the area that are necessary to cover the target heating load are found as 6 and 10 m$^2$ for the theoretical case. On the other hand, it is found from experimental investigation that, 9 SAHs with 16 m$^2$ are required. It is seen that there is disagreement between the theoretical (simulations) and experimental results. The disagreement is thought to be generated by the following reasons:

1) In the experimental setup the exit air from the SAH is exposed directly to the ambient. This is likely to reduce the exit air temperature for the experimental case, causing discrepancy between the theoretical and experimental results.

2) Thermal properties of the materials that are employed for manufacturing the SAH should be investigated in detail thus reducing the possible mismatch between the actual properties and those used for the theoretical evaluations.

3) The accuracies of the employed measuring equipment may generate noteworthy uncertainties in the experimental results thus equipment having better accuracies can be used.

Consequently, 9 of the V-Corrugated SAHs can be coupled together for covering the heating demand of the considered office space. It is also recommended that the simulations for obtaining the required number of SAHs for covering the demand for the space should be used with care as they are resulting in larger useful heat which gives a smaller number of SAHs.

It is suggested that in any case an auxiliary heater should be employed for the days having not enough solar radiation.

## ACKNOWLEDGMENTS

This work is produced from the Master of Science Thesis of Mr. Khaled Alteer, titled "Installation and Performance Testing of Solar Air Heater for Office Heating" which was presented in the Department of Mechanical Engineering of Eastern Mediterranean University in 2017 (Alteer, 2017).

The first author of the current work finds this opportunity to acknowledge the efforts of Mr. Khaled Alteer during his studies and would like to thank for his contribution to the current work.

## REFERENCES

Agathokleous R., Barone G., Buonomano A., Forzano C., Kalogirou S. A. and Palombo A, 2019, Building Facade Integrated Solar Thermal Collectors For Air

Heating: Experimentation, Modelling and Applications, *Applied Energy*, 239, 658–679.

Al-Kayiem H. H. and Yassen T. A., 2015, On the Natural Convection Heat Transfer in a Rectangular Passage Solar Air Heater, *Solar Energy*, 112, 310–318.

Alteer K., 2017, *Installation and Performance Testing of Solar Air Heater for Office Heating*, M.Sc. Thesis Eastern Mediterranean University, Famagusta.

ASHRAE, 2017, *ASHRAE Fundamentals 2017,* (SI Edition), ASHRAE, Atlanta.

Bayrak F. and Oztop H. F., 2015, Experimental Analysis of Thermal Performance of Solar Air Collectors with Aluminum Foam Obstacles. *J. of Thermal Science and Technology*, 35, 11–20.

CIBSE, 2015, *Environmental design CIBSE Guide A*, (Eighth Edition), The Chartered Institution of Building Services Engineers, London.

Çiftçi E., Khanlari A., Sözen A., Aytaç İ. and Tuncer, A. D., 2021, Energy And Exergy Analysis Of A Photovoltaic Thermal (PVT) System Used In Solar Dryer: A Numerical and Experimental Investigation, *Renewable Energy*, 180, 410–423.

Duffie J. A., Beckman W. A. and Blair N., 2020. *Solar Engineering of Thermal Processes, Photovoltaics and Wind,* (5th ed.), Wiley, New Jersey.

El-Sebaii A. A., Aboul-Enein S., Ramadan M. R. I., Shalaby S. M. and Moharram B. M., 2011, Thermal Performance Investigation of Double Pass-Finned Plate Solar Air Heater, *Applied Energy*, 88(5), 1727–1739.

Fan W., Kokogiannakis G. and Ma Z., 2019a, Optimisation of Life Cycle Performance of a Double-Pass Photovoltaic Thermal-Solar Air Heater with Heat Pipes, *Renewable Energy*, 138, 90–105.

Fan W., Kokogiannakis G. and Ma Z., 2019b, Integrative Modelling and Optimisation of a Desiccant Cooling System Coupled with a Photovoltaic Thermal-Solar Air Heater, *Solar Energy*, 193, 929–947.

Fan W., Kokogiannakis G., Ma, Z. and Cooper P., 2017, Development of a Dynamic Model for a Hybrid Photovoltaic Thermal Collector – Solar Air Heater with Fins. *Renewable Energy*, 101, 816–834.

Gao W., Lin W., and Lu E., 2000, Numerical Study on Natural Convection Inside the Channel Between the Flat-Plate Cover and Sine-Wave Absorber of a Cross-Corrugated Solar Air Heater, *Energy Conversion and Management*, 41, 145–151.

Gawande V. B., Dhoble A. S., Zodpe, D. B. and Chamoli S., 2016. Experimental and CFD Investigation of Convection Heat Transfer in Solar Air Heater with Reverse L-Shaped Ribs. *Solar Energy*, 131, 275–295.

Gilani S. E., Al-Kayiem,H. H., Woldemicheal D. E., and Gilani S. I., 2017, Performance Enhancement of Free Convective Solar Air Heater by Pin Protrusions on yhe Absorber. *Solar Energy*, 151, 173–185.

Hedayatizadeh M., Sarhaddi F., Safavinejad A., Ranjbar F. and Chaji H., 2016, Exergy Loss-Based Efficiency Optimization of a Double-Pass/Glazed V-Corrugated Plate Solar Air Heater. *Energy*, 94, 799–810.

Holman J. P., 2012, *Experimental Methods for Engineers* (Eighth Edition), McGraw-Hill, New York.

Internet, 2021, International Energy Agency, *World Energy Outlook 2021*, www.iea.org/weo.

Jain D. and Jain R. K., 2004, Performance Evaluation of an Inclined Multi-Pass Solar Air Heater with In-Built Thermal Storage on Deep-Bed Drying Application. *Journal of Food Engineering*, 65(4), 497–509.

Kareem M. W., Habib K., Ruslan M. H. and Saha B. B., 2017, Thermal Performance Study of a Multi-Pass Solar Air Heating Collector System for Drying of Roselle (Hibiscus Sabdariffa). *Renewable Energy*, 113, 281–292.

Internet, 2021, kıb-tek (*Kıbrıs Türk Elektrik Kurumu*), Production-Consumption Statistics, https://www.kibtek.com/statistikler/.

Kumar A., Singh A. P., Akshayveer and Singh O. P., 2022, Performance Characteristics of a New Curved Double-Pass Counter Flow Solar Air Heater. *Energy*, 239.

Lin W., Gao W. and Liu T., 2006, A Parametric Study on the Thermal Performance of Cross-Corrugated Solar Air Collectors. *Applied Thermal Engineering*, 26(10), 1043–1053.

Liu T., Lin W., Gao W. and Xia, C., 2007, A Comparative Study of the Thermal Performances of Cross-Corrugated And V-Groove Solar Air Collectors, *International Journal of Green Energy*, 4(4), 427–451.

Internet, 2022, North Cyprus Meteorological Office, *Cyprus Climate*. General Weather of North Cyprus, http://kktcmeteor.org/meteorolojikbilgi/kibris-iklimi#

Prakash O., Kumar A., Samsher Dey K. and Aman A., 2022, Exergy and Energy Analysis of Sensible Heat Storage Based Double Pass Hybrid Solar Air Heater, *Sustainable Energy Technologies and Assessments*, 49.

Sahebari R., Enesi V. and Tamer U., 2013, *Designing and Manufacturing of a Solar Air Heater*, B.Sc. Thesis, Eastern Mediterranean University, Famagusta.

Sparrow E. M., and Lin S. H., 1962, Absorption of Thermal Radiation in A V-Groove Cavity, *International Journal of Heat and Mass Transfer*, 5(11), 1111–1115.

Turkish Standards Institute, 2008, *TSE 825 Thermal Insulation Requirements for Buildings*. Turkish Standards Institute, Ankara.

U.S. Department of Energy, 2016a, *EnergyPlus™ Version 8.6 Documentation Engineering Reference*, U.S. Department of Energym, Berkeley.

U.S. Department of Energy, 2016b, *EnergyPlus™ Version 8.6 Documentation Getting Started*, U.S. Department of Energy, Berkeley.

U.S. Department of Energy, 2016c, *EnergyPlus™ Version 8.6 Documentation Input Output Reference* (Version 8.6), U.S. Department of Energy, Berkeley.

Yildirim C., and Solmuş, İ., 2014, Investigaton of Double Pass Solar Air Collector Channel Depth on Thermohydraulic Efficiency. *J. of Thermal Science and Technology*, 34, 111–122.